

Roles of Sc and Ag Microalloying Elements in the Mechanical Properties of Al-Zn-Mg-Cu (Al7xxx) Alloy

Sung-Jae Won ^{1,2}, Hyeongsu So ^{1,2}, Jung-Woo Han ^{1,2}, Soong Ju Oh ² and Kyou-Hyun Kim ^{1,*}

¹ Korea-Russia Innovation Center, Korea Institute of Industrial Technology, Incheon 21655, Republic of Korea

² Department of Materials Science and Engineering, Korea University, Seoul 02841, Republic of Korea

* Correspondence: khkim1308@kitech.re.kr; Tel.: +82-32-226-1360

Abstract: In this study, we use microstructural investigation to examine the effects of Sc and Ag microalloying elements on the mechanical properties of Al-Zn-Mg-Cu-based (7050) alloy. Macroscopically, Sc and Ag microalloying elements significantly reduce the formation of intermetallic particles of S (Al₂CuMg) and T (Mg₃₂(Al, Zn)₄₉) and of stable η (MgZn₂) phase in Al7050 alloy. In addition, Sc microalloying element facilitates the precipitation of the η' (MgZn₂) hardening phase, while Ag microalloying element impedes the formation of the η' (MgZn₂) hardening phase. As a result, trace addition of Sc enhances the σ_{UTS} value of the Al7050 alloy from 552 MPa to 594 MPa without lowering the elongation of the Al7050 alloy (15.0% \rightarrow 15.5%). In contrast, the tensile strength of the Al7050 alloy decreases from 552 MPa to 456 MPa with the addition of Ag microalloying element, while the elongation increases from 15.0% to 21.0%.

Keywords: 7xxx series aluminum alloy; mechanical properties; microalloying



Citation: Won, S.-J.; So, H.; Han, J.-W.; Oh, S.J.; Kim, K.-H. Roles of Sc and Ag Microalloying Elements in the Mechanical Properties of Al-Zn-Mg-Cu (Al7xxx) Alloy. *Metals* **2023**, *13*, 244. <https://doi.org/10.3390/met13020244>

Academic Editors: Ying Chen and Nan Hu

Received: 2 January 2023

Revised: 25 January 2023

Accepted: 25 January 2023

Published: 27 January 2023



Copyright: © 2023 by the authors. Licensee MDPI, Basel, Switzerland. This article is an open access article distributed under the terms and conditions of the Creative Commons Attribution (CC BY) license (<https://creativecommons.org/licenses/by/4.0/>).

1. Introduction

To develop Al alloys, post-treatment processes are used to control microstructures of as-cast Al alloys. Microstructural change followed by post-treatment processes is a critical step in determining the mechanical properties of as-cast Al alloys. As a result, a variety of post-treatment processes have been proposed to improve the mechanical properties of Al alloys [1,2]. Among several post-treatments, thermomechanical processing is the most typically used method to optimize the mechanical properties of Al alloys; such processing in general consists of combinations of quenching, homogenization, solutionization, plastic working, and aging [3,4]. Mechanical properties of Al alloys are then controlled by the condition of thermomechanical processing. This can result in various mechanical properties even for the same Al alloys. Nevertheless, thermomechanical processing is mostly governed by the nature of Al alloys, so the degree of potential mechanical properties is limited once the Al alloy composition is determined [5,6].

Another technique of microalloying directly affects the nature of Al alloys, so as to accelerate the microstructural evolution during solidification and thermomechanical processing [7,8]. This microalloying technique thus provides a further chance to enhance the mechanical properties of Al alloys. Among several microalloying elements, Sc and Ag are most frequently introduced to develop high strength Al alloys of Al-Cu-Mg (2xxx series) [9,10] and Al-Zn-Mg-Cu (7xxx series) [11,12]. Trace additions of Sc are known to form Al₃M-type (M: Zr, Sc) phases at early stages of solidification in Al-Zn-Mg-Cu (7xxx series) [13–15]; these additions are responsible for Al grain refinement because they provide heterogeneous nucleation sites during the solidification stage [16]. On the other hand, a small addition of Sc has been reported to improve the strength of Al alloys, not by refining the Al grain, but by providing a high volume fraction of fine dispersoids [17]. Earlier reports, therefore, suggest that the effects of Sc microalloying element can vary with the composition of Al-Zn-Mg-Cu alloys.

Ag microalloying addition is mainly used to promote the formation of Ω precipitates in Al alloys of Al-Cu-Mg (2xxx series) [18,19]. For Al-Cu-Mg alloy systems, small amounts of Ag addition induce the formation of Ω phase on the closed-packed plane of $\{111\}_{Al}$. For Al-Zn-Mg-Cu series alloys, however, some studies have shown that the mechanical properties of Al-Zn-Mg-Cu-Ag alloys can vary with the thickness of the casting alloys [20]. In Al-Zn-Mg-Cu-Ag alloys, the exact role of Ag in the early stages of ageing, and the possible interaction between Ag and Cu atoms, remain unclear. To address the above questions, the ageing behaviors of Al-Zn-Mg-Cu alloys were investigated and microstructure evolution during the early stages of ageing was discussed with respect to the influence of Ag on precipitation [11,21].

Lightweight Al7050 alloy is of importance in the aerospace and transportation industries because of its high mechanical performances. Al7050 alloy is mainly strengthened by precipitate hardening of $MgZn_2$ phase with typical thermo-mechanical treatment [22,23]. The commercial Al7050 plate is known to possess a high tensile strength of ~ 570 MPa. As mentioned, the mechanical performances of Al7050 can be further enhanced by microalloying techniques using Sc and Ag. In this study, Sc and Ag microalloying elements changed the mechanical properties of Al7050. The Sc elements improved the mechanical properties of Al7050 alloy from 552 to 594 MPa. Interestingly, the addition of Sc microalloying element reduced the formation of large intermetallic compounds in the grain boundary regions and facilitated the growth of hardening precipitates. Similarly, the addition of Ag element also reduced the formation of large intermetallic particles in the Al grain boundaries. The hardening precipitates of $MgZn_2$, however, entirely disappeared after the addition of Ag element. This resulted in a decrease in mechanical strength and an increase in plasticity. Interestingly, the observed effects of Sc and Ag microalloying elements have hardly been reported on for Al7xxx alloys. This study, therefore, performed microstructural investigation from the microscopic to the macroscopic scale to determine the effects of Sc and Ag microalloying on the mechanical properties of the Al7050 alloy.

2. Experimental Procedures

Chemical compositions of the investigated Al-Zn-Mg-Cu-based alloys are given in Table 1. High-purity metal elements of Al (99.99%), Zn (99.99%), Mg (99.99%), Ag (99.99%), and Al-Sc (98:2%) master alloys were melted using a high-frequency induction furnace (DY Induction Ltd., Incheon, Korea) at 800 °C; other minor elements were added to the molten metal for homogenous mixing. During melting, Ar gas was injected into the molten metal for 15 min to remove residual induced pores. The molten metal was then cast into molds (SKD-61, 120.0 mm \times 60.0 mm \times 30.0 mm). For casting, the mold temperature was maintained at 200 °C. As shown in Table 1, trace amounts of Sc and Ag elements were added to commercial Al7050 alloy. Hereinafter, conventional Al7050, Sc-added, and Ag-added Al7050 alloys will be referred to as Al7050, Al7050-Sc, and Al7050-Ag, respectively. The as-cast samples were T6 tempered based on conventional conditions of homogenization (470 °C/24 h) \rightarrow hot rolling (reduction ratio: 70%) \rightarrow solutionization (470 °C/2 h, water quenching) \rightarrow artificial aging (120 °C/24 h) [24]. Mechanical tensile tests were carried out using a universal testing machine (UTM, AG-300kNx plus, Shimadzu Co., Kyoto, Japan) according to ASTM standard E-8M. Test specimens were taken along the rolling direction (RD) and had gauge lengths of 25 mm. These samples were then stretched with a constant extension rate (1 mm/min) at room temperature. Tensile testing was performed more than 10 times for every specimen to obtain an average value. The mechanical properties of Al7050 alloys are known to be independent of the natural aging process [25]. Nevertheless, all samples were investigated within ~ 7 days of the artificial aging process. Origins of the mechanical properties were discussed based on microstructural investigations obtained by optical microscopy (OM), secondary electron microscopy (FE-SEM, JSM-7100F, JEOL Ltd., Tokyo, Japan), and X-ray diffraction (XRD, D8 ADVANCE, Bruker Corp., Billerica, MA, USA). Details at nanoscopic scale were then obtained using field-emission transmission electron microscopy (FE-TEM, Tecnai F20 SuperTwin, FEI). For the TEM study, the speci-

mens were mechanically polished down to $\sim 20 \mu\text{m}$ and Ar-ion milled (PIPSTM, Precision Ion Polishing System, GATAN Inc., Pleasanton, CA, USA) at an incident angle of 6° with an accelerating voltage of 3.0 keV for electron transparency.

Table 1. Nominal compositions of the designed alloys.

Alloys	Chemical Composition (wt.%)							
	Al	Zn	Mg	Cu	Cr	Zr	Sc	Ag
Al7050	Bal.	6.4	2.2	2.2	0.14	0.08	-	-
Al7050-Sc	Bal.	6.4	2.2	2.2	0.14	0.08	0.1	-
Al7050-Ag	Bal.	6.4	2.2	2.2	0.14	0.08	-	0.1

3. Results

Figure 1 shows the tensile properties of the T6-tempered Al7050, Al7050-Sc, and Al7050-Ag alloys. The Al7050 alloy has a σ_{UTS} of 552 MPa, with elongation of $\sim 15.0\%$. Indeed, the measured tensile properties are almost identical to the reported values of the commercial Al7050 alloy [23]. As shown in Figure 1, the microalloying elements Sc and Ag have different effects on the tensile properties of the Al7050 alloy. First, the addition of a trace amount of Sc enhances the σ_{UTS} value of the Al7050 alloy from 552 MPa to 594 MPa without lowering the elongation of the Al7050 alloy ($15.0\% \rightarrow 15.5\%$). In contrast, with trace addition of the Ag microalloying element, the σ_{UTS} value of the Al7050 alloy decreases from 552 MPa to 456 MPa. Instead, the elongation greatly improves from 15.0% to 21.0% . The role of Sc and Ag microalloying elements will be discussed next based on microstructural investigation.

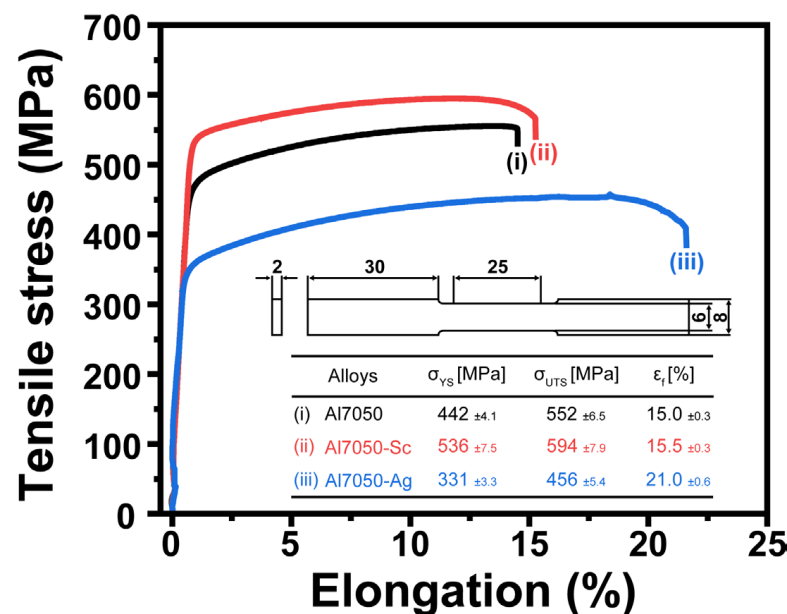


Figure 1. Tensile stress–strain curves obtained from T6-tempered (120°C , 24 h) Al7050, Al7050-Sc, and Al7050-Ag alloys.

Figure 2 shows the XRD profiles of 2θ scans recorded from the Al7050, Al7050-Sc, and Al7050-Ag alloys. The recorded XRD profiles consist of strong major peaks of α -Al (FCC, $\text{Fm}\bar{3}\text{m}$), with several minor peaks. For the Al7050 alloy, the minor peaks are identified as MgZn_2 (η or η' phase, HCP, $\text{P}6_3/\text{mmc}$), Al_2CuMg (S phase, Cmcm), and $\text{Mg}_{32}(\text{Al}, \text{Zn})_{49}$ (T phase, $\text{Im}\bar{3}$) [15,26,27]. Based on earlier reports, the S and T phases preferentially precipitated at grain boundaries of the Al7xxx alloy system [28,29]. For the Al7050-Sc alloy, the peaks observed in the XRD profiles are almost identical to that of the Al7050 alloy. The peaks of η (or η'), S, and T phases are well defined for the Al7050-Sc alloy, as shown in

Figure 2b. The peak intensities of η (or η'), S, and T phases, however, significantly decrease in the XRD profile of the Al7050-Sc alloy. For the Ag microalloying element, the peak intensities of S, T, and η (or η') phases further decrease in the Al7050-Ag alloy compared with those of Al7050 and Al7050-Sc alloys, as shown in Figure 2c.

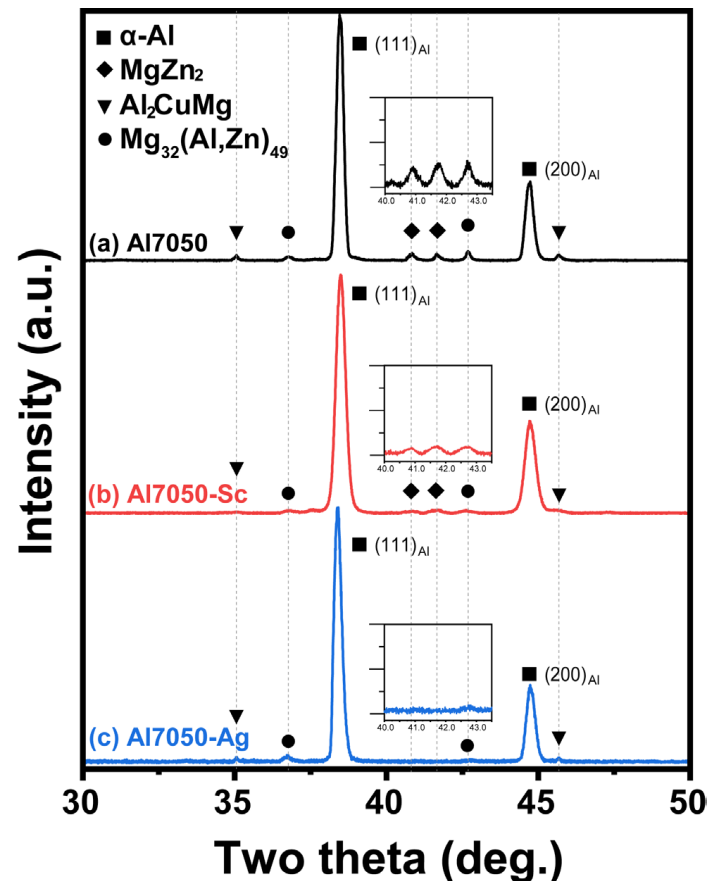


Figure 2. XRD profiles of (a) Al7050, (b) Al7050-Sc, and (c) Al7050-Ag.

Figure 3 shows typical back-scattered electron (BSE) images of the investigated alloys. We confirmed that the microstructure of the investigated specimens is very homogeneous regardless of sample positions. The EDS analysis was carried out in at least five different areas to obtain the averaged elemental ratios. As shown in Figure 3a, the Al7050 alloy mainly consists of Al grains with intermetallic particles inside the Al grain (inset of Figure 3a) and at the grain boundaries (dotted-box). The observed intermetallic compounds can be then divided into two groups with respect to their size. The large intermetallic particles are 10–20 μm , while the fine intermetallic particles are less than a few μm (inset of Figure 3a). According to the chemical analysis (Table 2), the observed large intermetallic particles (I) are mainly composed of Zn/Mg/Cu, while the fine intermetallic particles (II) consist of Zn/Mg. Compared with the XRD indexing results, therefore, the large intermetallic particles are considered to be S (Al_2CuMg) and T ($\text{Mg}_{32}(\text{Al}, \text{Zn})_{49}$) phases [28,29], while the small intermetallic particle is revealed to be stable η (MgZn_2) phase [30,31]. These intermetallic phases, however, are greatly affected by trace additions of Sc and Ag. As shown in Figure 3b,c, the fractions of intermetallic particles obviously decrease in both Al7050-Sc and Al7050-Ag alloys, which agree well with the XRD results. Especially, the small intermetallic compounds of stable η (MgZn_2) phase almost disappear in both Al7050-Sc and Al7050-Ag alloys. For the large particles observed in the Al7050-Sc alloy, the chemical analysis (I') reveals that the main elements are Zn/Mg/Cu, the same large particles found in the Al7050 alloy. Considering XRD identification, therefore, the large intermetallic compounds observed in the Al7050-Sc alloy can also be defined as S (Al_2CuMg) and T ($\text{Mg}_{32}(\text{Al}, \text{Zn})_{49}$)

phases. Similarly, the large particles (I'') observed in the Al7050-Ag alloy are identified as T phase with a small amount of S phase. Based on the recorded BSE images, therefore, trace addition of Ag further restricts the formation of T ($Mg_{32}(Al, Zn)_{49}$) and S (Al_2CuMg) phase compared with the Sc microalloying element, resulting in a significant decrease in the fraction of large particles in the Al7050-Ag alloy, as shown in Figure 3c.

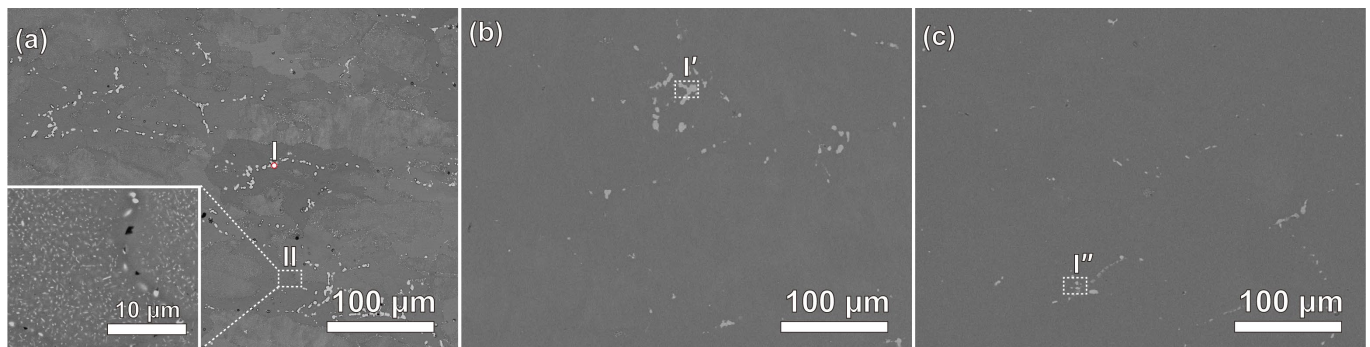


Figure 3. Typical BSE images of (a) Al7050, (b) Al7050-Sc, and (c) Al7050-Ag.

Table 2. Chemical investigations of intermetallic particles, as shown in Figure 3.

	Atomic %			
	Al	Zn	Mg	Cu
(a) Al7050—I	50.6	1.8	23.1	24.5
(b) Al7050—II	92.4	3.1	3.6	0.9
(c) Al7050-Sc—I'	48.1	2.2	20.3	29.4
(d) Al7050-Ag—I''	74.5	1.2	12.5	11.8

Figure 4 shows phase contrast images of Al grains recorded from synthesized Al alloys. First, as shown in Figure 4a, uniformly distributed dark contrasts are observed in the Al grain of Al7050, as indicated by an arrow. These nanosized uniform contrasts resulted from coherent pre-precipitates (GP-zone) generated by the coherent misfit strain perpendicular to the observation axis of $[110]_{Al}$. As shown in the inset of Figure 4a, the diffuse streaks along the $g_{\{111\}}$ of Al also indicate that the Al matrix has planar faults in the GP-zone. In the Al7050 alloy, the number density of precipitates (GP-zone) is calculated at 3.8×10^4 counts/ μm^2 . For the Al7050-Sc alloy, the representative phase contrast image shows that the pre-precipitates found in Al7050 grew to ~ 1 nm thick and ~ 6.4 nm in diameter with trace addition of Sc. On the other hand, the number density of precipitates decreased to 2.1×10^4 counts/ μm^2 in the Al7050-Sc alloy. Similar to the Al7050 alloy, the existence of fine precipitates formed streaks in the electron diffraction pattern. As shown in the inset of Figure 4b, the electron spot of $\frac{1}{3}g_{(220)}_{Al}$ provides direct evidence for the formation of metastable η' ($MgZn_2$) phase [30]. Furthermore, extra precipitates spots are found at $\frac{1}{2}g_{(220)}_{Al}$ of Al, which indicates the formation of Al_3M (M: Sc, Zr) phase. The Al_3M phase typically forms in spherical shape [32], as indicated in Figure 4b. In contrast, the trace addition of Ag hinders the formation of hardening precipitates in the Al matrix, as expected from the XRD results (Figure 2). As shown in Figure 4c, the major hardening precipitates of η or η' phase are not observed in the Ag-microalloyed Al7050 alloy.

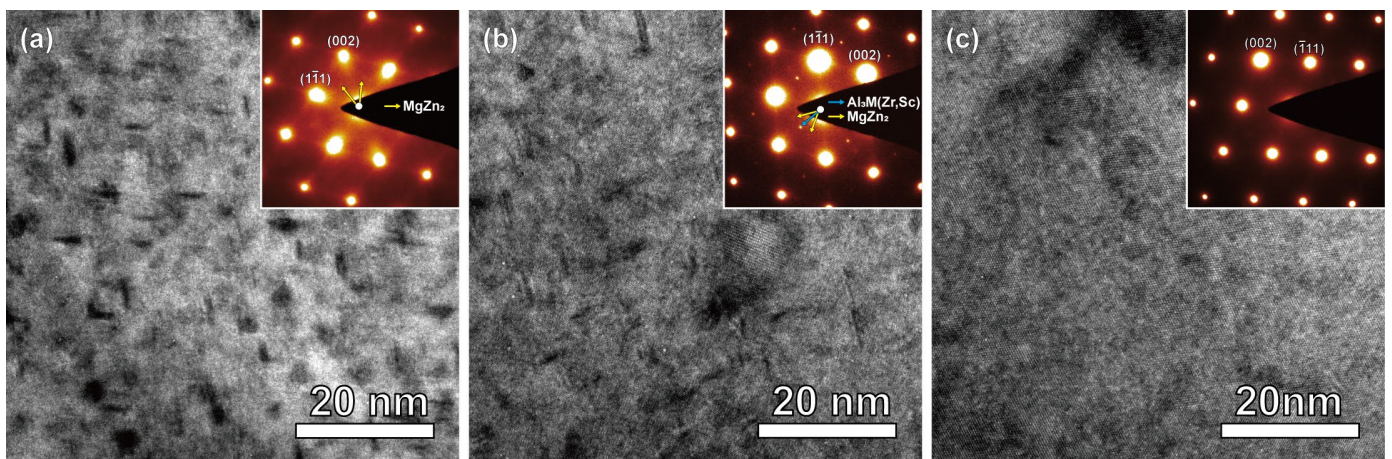


Figure 4. Bright-field images and corresponding electron diffraction patterns recorded from (a) Al7050, (b) Al7050-Sc, and (c) Al7050-Ag.

4. Discussion

Microstructural investigation showed that trace additions of Sc and Ag induce microstructural evolution in the Al7050 alloy. The microstructural evolution can then be discussed in the aspects of macroscopic and nanoscopic scale. For the macroscopic scale, using SEM with the help of XRD identification, the major phases of η , S, and T are observed in the Al7050 alloy. The stable η phase is mostly observed inside the Al grain, while the S and T phases are only found at the grain boundaries of Al. On the other hand, the pre-precipitates (GP-zone) are observed in the Al grain of Al7050 at nanoscopic scale.

The macroscopic and nanoscopic microstructural features change dramatically with the addition of trace amounts of Sc and Ag to the commercial Al7050 alloy. The first remarkable microstructural change is the stable η phase. The stable η phase almost disappears in both Al7050-Sc and Al7050-Ag alloys. Furthermore, the volume fractions of large secondary intermetallic S (Al_2CuMg) and T ($\text{Mg}_{32}(\text{Al}, \text{Zn})_{49}$) particles significantly decrease in the Al7050-Sc and Al7050-Ag alloys. The above experimental results, therefore, suggest that more minor elements of Zn-Mg-Cu exist in the Al grain by the addition of Sc and Ag microalloying elements. Especially, compared with the Sc microalloying element, the Ag microalloying element seems to be more effective at deriving the existence of Zn-Mg-Cu minor elements in the Al grain because the S and T phases dramatically decrease in the Al7050-Ag alloy. Consequently, it can be reasonably accepted that the increase in minor elements in the Al grain necessarily results in increases in hardening precipitates in the Al grain [33,34]. Precipitates' formation, however, follows different processes for the Sc and Ag microalloying elements.

For the Al7050 alloy, stable MgZn_2 (η) particles and pre-precipitates (GP-zones) are mainly formed inside the Al grain under peak aging (T6) condition. On the other hand, the Sc-microalloyed Al7050 alloy is only composed of metastable η' precipitates in the Al matrix, without the formation of a stable η phase even at the same peak aging condition. This, therefore, gives direct evidence that the Sc microalloying element facilitates the precipitate formation process of GP-zone \rightarrow metastable η' phase, while the Sc element restricts the precipitate formation process of metastable η' phase \rightarrow stable η phase. This could be the result of the increase in solid solution element in the Al matrix by trace addition of Sc. On the other hand, the Ag microalloying element impedes any formation of hardening precipitates in the Al grain of the Al7050 alloy, while the Al7050-Ag alloy, among the investigated Al alloys, is considered to possess most abundant minor elements of Zn/Mg/Cu in the Al grain.

The above microstructural evolutions directly affect the mechanical strength of the Al7050 alloy. Tensile tests of the Al7050-Sc alloy demonstrated that the mechanical strength of the Al7050 alloy can be effectively enhanced by formation of metastable η' phase, a major

hardening precipitate in the Al7xxx series alloy [35,36]. Trace Sc addition improves the value of σ_{UTS} of the Al7050 alloy from 552 MPa to 594 MPa. Additionally, Sc microalloying reduces the volume fraction of large intermetallic particles at grain boundaries of Al, which in general act as crack initiation sites [12,37]. Elongation of the Al7050-Sc alloy shows a value similar to that of the Al7050 ($\epsilon = \sim 15\%$) alloy, even though the tensile strength increases in the Al7050-Sc ($\epsilon = \sim 15.5\%$) alloy. On the other hand, the tensile strength of the Al7050-Ag alloys decreases dramatically from 552 MPa to 456 MPa. This is due to the absence of hardening precipitates in the Al matrix. Otherwise, decreases in hardening precipitates and large intermetallic particles at the grain boundaries resulted in increases in elongation from $\sim 15.0\%$ (Al7050) to 21.0% (Al7050-Ag).

Interestingly, this study demonstrated that Ag microalloying hinders the formation of η' phase in the Al7050 alloy, while the trace addition of Ag enhances the formation of Ω (Al₂Cu) phase on the closed packed plane of $\{111\}_{Al}$ in Al-Cu-Mg (2xxx series) alloys [38]. The previous study involving a three-dimensional atom probe (3DAP) revealed that Ag-Mg co-clusters were induced in the early stage of pre-precipitation, pushing the formation of Ω precipitates by incorporating Cu atoms [9]; Ag and Mg segregation finally exists at the $\{111\}$ Ω/α interfaces. In consequence, it is expected that the strong interaction between Ag-Mg co-clusters impedes the formation of MgZn₂ phase in the investigated Al7050 alloy.

5. Conclusions

In this study, we demonstrated the effect of Sc and Ag microalloying elements on the mechanical properties of the Al7050 alloy. Compared with the Al7050 alloy, the Sc microalloying alloy enhanced the mechanical properties, to a value of $\sigma_{UTS} = 594$ MPa ($\epsilon = 15.5\%$) from $\sigma_{UTS} = 552$ MPa for Al7050. On the other hand, Ag microalloying lowered the tensile strength from a value of $\sigma_{UTS} = 552$ MPa (Al7050) to $\sigma_{UTS} = 456$ MPa, while the elongation significantly increased from $\epsilon = 15.0\%$ to $\epsilon = 21.0\%$. In earlier reports, the conventional role of Sc microalloying element is known to be that of a grain refiner. In addition, Ag microalloying elements are in general known to facilitate the formation of Ω phase. This study, however, demonstrated that the Sc and Ag microalloying elements directly caused the formation of large intermetallic particles and hardening precipitates in the Al grain, resulting in different mechanical properties, as follows:

- (1) Sc and Ag microalloying elements impede the formation of intermetallic particles (S, T, η phases) in Al7050 alloys.
- (2) Sc microalloying element facilitates the precipitate formation process of the GP-zone \rightarrow metastable η' phase, while the process of metastable η' phase \rightarrow stable η phase is severely restricted. The formation of hardening η' phase greatly improves the tensile strength of the Al7050 alloy.
- (3) The major hardening precipitates of η' (MgZn₂) phase are restricted to form in the Al7050 alloy via Ag microalloying.

Author Contributions: Data curation, S.-J.W. and H.S.; Funding acquisition, K.-H.K.; Investigation, S.-J.W., H.S., and J.-W.H.; Resources, S.J.O. and K.-H.K.; Supervision, S.J.O. and K.-H.K.; Writing—original draft, S.-J.W.; Writing—review and editing, K.-H.K. All authors have read and agreed to the published version of the manuscript.

Funding: This research was financially supported by the Institute of Civil Military Technology Cooperation, funded by the Defense Acquisition Program Administration and the Ministry of Trade, Industry, and Energy of the Korean Government, under grant No. UM21308RD3.

Institutional Review Board Statement: Not applicable.

Informed Consent Statement: Not applicable.

Data Availability Statement: The raw/processed data required to reproduce these findings cannot be shared at this time as the data also form part of an ongoing study.

Acknowledgments: This study was also partially supported by the R&D program and research facilities of the Korea Institute of Industrial Technology.

Conflicts of Interest: The authors declare no conflict of interest.

References

1. Embury, J.; Nicholson, R. The nucleation of precipitates: The system Al-Zn-Mg. *Acta Metall.* **1965**, *13*, 403–417. [[CrossRef](#)]
2. Chen, Y.; Gao, N.; Sha, G.; Ringer, S.P.; Starink, M.J. Microstructural evolution, strengthening and thermal stability of an ultrafine-grained Al-Cu-Mg alloy. *Acta Mater.* **2016**, *109*, 202–212. [[CrossRef](#)]
3. Marlaud, T.; Deschamps, A.; Bley, F.; Lefebvre, W.; Baroux, B. Influence of alloy composition and heat treatment on precipitate composition in Al-Zn-Mg-Cu alloys. *Acta Mater.* **2010**, *58*, 248–260. [[CrossRef](#)]
4. Starink, M.; Wang, S. A model for the yield strength of overaged Al-Zn-Mg-Cu alloys. *Acta Mater.* **2003**, *51*, 5131–5150. [[CrossRef](#)]
5. Zuo, J.; Hou, L.; Shu, X.; Peng, W.; Yin, A.; Zhang, J. Grain refinement assisted by deformation enhanced precipitates through thermomechanical treatment of AA7055 Al alloy. *Metals* **2020**, *10*, 594. [[CrossRef](#)]
6. Zuo, J.; Hou, L.; Shi, J.; Cui, H.; Zhuang, L.; Zhang, J. The mechanism of grain refinement and plasticity enhancement by an improved thermomechanical treatment of 7055 Al alloy. *Mater. Sci. Eng. A* **2017**, *702*, 42–52. [[CrossRef](#)]
7. Liu, J.; Yao, P.; Zhao, N.; Shi, C.; Li, H.; Li, X.; Xi, D.; Yang, S. Effect of minor Sc and Zr on recrystallization behavior and mechanical properties of novel Al-Zn-Mg-Cu alloys. *J. Alloys Compd.* **2016**, *657*, 717–725. [[CrossRef](#)]
8. Wu, Y.-L.; Li, C.; Alvarez, A. Microalloying of Sc, Ni, and Ce in an advanced Al-Zn-Mg-Cu alloy. *Metall. Mater. Trans. A* **1999**, *30*, 1017–1024. [[CrossRef](#)]
9. Reich, L.; Murayama, M.; Hono, K. Evolution of Ω phase in an Al-Cu-Mg-Ag alloy—A three-dimensional atom probe study. *Acta Mater.* **1998**, *46*, 6053–6062. [[CrossRef](#)]
10. Gazizov, M.; Teleshov, V.; Zakharov, V.; Kaibyshev, R. Solidification behaviour and the effects of homogenisation on the structure of an Al-Cu-Mg-Ag-Sc alloy. *J. Alloys Compd.* **2011**, *509*, 9497–9507. [[CrossRef](#)]
11. Zhu, Q.; Cao, L.; Wu, X.; Zou, Y.; Couper, M.J. Effect of Ag on age-hardening response of Al-Zn-Mg-Cu alloys. *Mater. Sci. Eng. A* **2019**, *754*, 265–268. [[CrossRef](#)]
12. Ying, T.; Gu, L.; Tang, X.; Wang, J.; Zeng, X. Effect of Sc microalloying on microstructure evolution and mechanical properties of extruded Al-Zn-Mg-Cu alloys. *Mater. Sci. Eng. A* **2022**, *831*, 142197. [[CrossRef](#)]
13. Freiberg, D.; Zhu, W.; Park, J.-S.; Almer, J.D.; Sanders, P. Precipitate characterization in model Al-Zn-Mg-(Cu) alloys using small-angle X-ray scattering. *Metals* **2020**, *10*, 959. [[CrossRef](#)]
14. Ogura, T.; Hirose, S.; Cerezo, A.; Sato, T. Atom probe tomography of nanoscale microstructures within precipitate free zones in Al-Zn-Mg (-Ag) alloys. *Acta Mater.* **2010**, *58*, 5714–5723. [[CrossRef](#)]
15. Zhang, M.; Liu, T.; He, C.; Ding, J.; Liu, E.; Shi, C.; Li, J.; Zhao, N. Evolution of microstructure and properties of Al-Zn-Mg-Cu-Sc-Zr alloy during aging treatment. *J. Alloys Compd.* **2016**, *658*, 946–951. [[CrossRef](#)]
16. Won, S.-J.; So, H.; Kang, L.; Oh, S.J.; Kim, K.-H. Development of a high-strength Al-Zn-Mg-Cu-based alloy via multi-strengthening mechanisms. *Scr. Mater.* **2021**, *205*, 114216. [[CrossRef](#)]
17. Yoganjaneyulu, G.; Babu, K.A.; Siva, G.V.; Vigneshwaran, S.; Narayanan, C.S. Microstructure and mechanical properties of Al-6 Zn-3 Mg-2 Cu-0.5 Sc alloy. *Mater. Lett.* **2019**, *253*, 18–21. [[CrossRef](#)]
18. So, H.; Won, S.-J.; Park, J.; Oh, S.J.; Kang, L.; Kim, K.-H. Mechanical properties and microstructural evolution in Al-Cu-Mg-Ag alloy with a CuxMgx/10 content. *Mater. Sci. Eng. A* **2021**, *824*, 141573. [[CrossRef](#)]
19. Li, B.; Liang, S.; Wen, S.; Zhao, Z.; Wu, X.; Wang, W.; Gao, K.; Huang, H.; Nie, Z. Competition between precipitation and segregation of Sc and its effects on thermal stability of Al-Cu-Mg-Ag alloys. *Mater. Lett.* **2021**, *297*, 129927. [[CrossRef](#)]
20. Staley, J.; Brown, R.; Schmidt, R. Heat treating characteristics of high strength Al-Zn-Mg-Cu alloys with and without silver additions. *Metall. Mater. Trans. B* **1972**, *3*, 191–199. [[CrossRef](#)]
21. Lin, L.; Liu, Z.; Liu, W.; Zhou, Y.; Huang, T. Effects of Ag addition on precipitation and fatigue crack propagation behavior of a medium-strength Al-Zn-Mg alloy. *J. Mater. Sci. Tec.* **2018**, *34*, 534–540. [[CrossRef](#)]
22. Chung, T.-F.; Yang, Y.-L.; Shiojiri, M.; Hsiao, C.-N.; Li, W.-C.; Tsao, C.-S.; Shi, Z.; Lin, J.; Yang, J.-R. An atomic scale structural investigation of nanometre-sized η precipitates in the 7050 aluminium alloy. *Acta Mater.* **2019**, *174*, 351–368. [[CrossRef](#)]
23. Sha, G.; Cerezo, A. Early-stage precipitation in Al-Zn-Mg-Cu alloy (7050). *Acta Mater.* **2004**, *52*, 4503–4516. [[CrossRef](#)]
24. Carvalho, A.; Renaudin, L.; Zara, A.; Martins, J. Microstructure analysis of 7050 aluminum alloy processed by multistage aging treatments. *J. Alloys Compd.* **2022**, *907*, 164400. [[CrossRef](#)]
25. Zhou, B.; Liu, B.; Zhang, S. The advancement of 7xxx series aluminum alloys for aircraft structures: A review. *Metals* **2021**, *11*, 718. [[CrossRef](#)]
26. Deng, Y.; Zhang, Y.; Wan, L.; Zhang, X. Effects of thermomechanical processing on production of Al-Zn-Mg-Cu alloy plate. *Mater. Sci. Eng. A* **2012**, *554*, 33–40. [[CrossRef](#)]
27. Kheradmand, A.B.; Tayebi, M.; Akbari, M.M.; Abbasian, A. Effect of quench-controlled precipitation hardening on microstructure and mechanical properties of Al-Zn-Mg-Cu-Zr alloys contain of Sc micro-alloying. *J. Alloys Compd.* **2022**, *902*, 163748. [[CrossRef](#)]
28. Zhao, Y.; Li, Y.; Yeli, G.; Luan, J.; Liu, S.; Lin, W.; Chen, D.; Liu, X.; Kai, J.; Liu, C. Anomalous precipitate-size-dependent ductility in multicomponent high-entropy alloys with dense nanoscale precipitates. *Acta Mater.* **2022**, *223*, 117480. [[CrossRef](#)]

29. Zou, Y.; Wu, X.; Tang, S.; Zhu, Q.; Song, H.; Cao, L. Co-precipitation of T' and η' phase in Al-Zn-Mg-Cu alloys. *Mater. Charact.* **2020**, *169*, 110610. [[CrossRef](#)]
30. Li, X.; Hansen, V.; Gjønnes, J.; Wallenberg, L. HREM study and structure modeling of the η' phase, the hardening precipitates in commercial Al-Zn-Mg alloys. *Acta Mater.* **1999**, *47*, 2651–2659. [[CrossRef](#)]
31. Fang, X.; Song, M.; Li, K.; Du, Y.; Zhao, D.; Jiang, C.; Zhang, H. Effects of Cu and Al on the crystal structure and composition of η (MgZn_2) phase in over-aged Al-Zn-Mg-Cu alloys. *J. Mater. Sci.* **2012**, *47*, 5419–5427. [[CrossRef](#)]
32. Novotny, G.M.; Ardell, A.J. Precipitation of Al₃Sc in binary Al-Sc alloys. *Mater. Sci. Eng. A* **2001**, *318*, 144–154. [[CrossRef](#)]
33. Zhang, Y.; Weyland, M.; Milkereit, B.; Reich, M.; Rometsch, P.A. Precipitation of a new platelet phase during the quenching of an Al-Zn-Mg-Cu alloy. *Sci. Rep.* **2016**, *6*, 23109. [[CrossRef](#)] [[PubMed](#)]
34. Dos Santos, J.F.; Staron, P.; Fischer, T.; Robson, J.D.; Kostka, A.; Colegrove, P.; Wang, H.; Hilgert, J.; Bergmann, L.; Hütsch, L.L. Understanding precipitate evolution during friction stir welding of Al-Zn-Mg-Cu alloy through in-situ measurement coupled with simulation. *Acta Mater.* **2018**, *148*, 163–172. [[CrossRef](#)]
35. Mazzer, E.; Afonso, C.; Galano, M.; Kiminami, C.; Bolfarini, C. Microstructure evolution and mechanical properties of Al-Zn-Mg-Cu alloy reprocessed by spray-forming and heat treated at peak aged condition. *J. Alloys Compd.* **2013**, *579*, 169–173. [[CrossRef](#)]
36. Ghiaasiaan, R.; Amirkhiz, B.S.; Shankar, S. Quantitative metallography of precipitating and secondary phases after strengthening treatment of net shaped casting of Al-Zn-Mg-Cu (7000) alloys. *Mater. Sci. Eng. A* **2017**, *698*, 206–217. [[CrossRef](#)]
37. Sun, Y.; Luo, Y.; Pan, Q.; Liu, B.; Long, L.; Wang, W.; Ye, J.; Huang, Z.; Xiang, S. Effect of Sc content on microstructure and properties of Al-Zn-Mg-Cu-Zr alloy. *Mater. Today Commun.* **2021**, *26*, 101899. [[CrossRef](#)]
38. Kang, S.J.; Kim, Y.-W.; Kim, M.; Zuo, J.-M. Determination of interfacial atomic structure, misfits and energetics of Ω phase in Al-Cu-Mg-Ag alloy. *Acta Mater.* **2014**, *81*, 501–511. [[CrossRef](#)]

Disclaimer/Publisher's Note: The statements, opinions and data contained in all publications are solely those of the individual author(s) and contributor(s) and not of MDPI and/or the editor(s). MDPI and/or the editor(s) disclaim responsibility for any injury to people or property resulting from any ideas, methods, instructions or products referred to in the content.